International Journal of Advancements in Mechanical and Aeronautical Engineering – IJAMAE 2018
Copyright © Institute of Research Engineers and Doctors , SEEK Digital Library
Volume 5 : Issue 2- [ISSN : 2372-4153] - Publication Date: 28 December, 2018

Calculation and Analysis of Dynamic Stress of High-Altitude Vehicle's Working Arms

[Yuxin Zheng Ying Xi Wanghui Bu]

***Abstract*—According to the working principle of a certain type of high-altitude vehicle, the force analysis of working arm of the high-altitude vehicle was carried out. Based on this, the working conditions of lifting, lowering, rotating, and luffing were simulated to consider the influence of the angle variation of luffing angle α and folding angle β on the stress of the working arm. Using MATLAB to draw the diagrams of the dynamic relationship between the stress and the amplitude luffing angle α and folding angle β , which provides a theoretical basis for the optimal design and life prediction of the working arm of a high-altitude vehicle.**

Keywords—high-altitude vehicle; force analysis; stress analysis; luffing angle; folding angle

I. Introduction

The working device of trailer-type high-altitude vehicle includes a basic arm and a primary arm of telescopic arm, a main arm and a auxiliary arm of folding-arm etc. As a modern advanced equipment for special purposes, the high-altitude vehicle has attracted extensive attention from scholars at home and abroad. In [1], Janusz Krasuckid and others from Poland conducted an in-depth study of the hybrid-powered high-altitude vehicle. They established a lift control model for the high-altitude vehicle. In [2], Giguere used the high-altitude vehicle to complete the rescue work, the strength of the force when the man jumped to the platform was studied, and several appropriate postures were suggested when the man jumped down. In [3] and [4], Timothy, B.Hale and others established the ADAMS simulation model of the high-altitude vehicle, and obtained the curves of the speed, acceleration and displacement of mass center. In [5], Hu Yuan analyzed five types of luffing mechanisms used in high-altitude vehicle, and compared their structure, working principle, and scope of application. In [6], Liu Jingang used ADAMS to simulate and optimize the luffing mechanism of high-altitude vehicle, and obtained the best luffing mechanism. In [7], Zhao Xuelong conducted a force calculation of the scissor mechanism of the high-altitude vehicle. It is dangerous for working at height, so it is important to ensure the safety of the operators. Finding the stress dangerous sections of each working arm is necessarily In this paper, the dynamic stress of each working arm is calculated accurately, and the dynamic stress curves are plotted, which provides a theoretical basis for the optimal design and life prediction of high-altitude vehicle.

Yuxin Zheng /PhD candidate
School of Mechanical Engineering, Tongji University
China

Ying Xi /Professor
School of Mechanical Engineering, Tongji University
China

Wanghui Bui /Professor
School of Mechanical Engineering, Tongji University
China

II. Basic Parameters of High-Altitude Vehicle

The schematic diagram of a high-altitude vehicle is shown in Fig. 1. According to Tab. 1, the maximum height reached by the high-altitude vehicle is 12.36 m, and the maximum horizontal distance is 5.59 m. According to the technical parameters in Tab. 1, the length of each arm and the stroke of telescopic arm can be accurately calculated, But the calculation process are not detailed described.

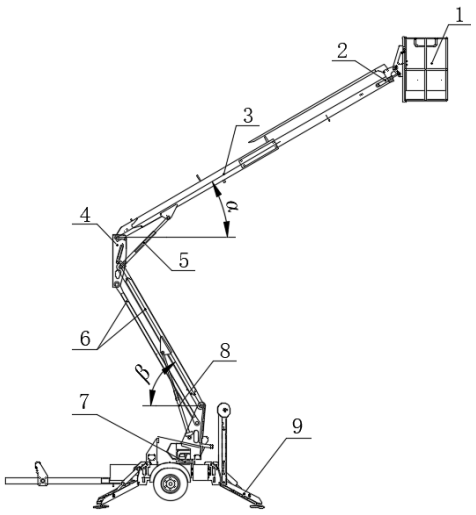

1. Working platform 2. Hydraulic cylinder 3. Telescopic arm 4. Connecting plate 5. Telescopic arm luffing cylinder 6. Double parallel folding arm 7. Slewing platform 8. Folding arm luffing cylinder 9. Legs

Figure 1. Schematic diagram of a high-altitude vehicle

TABLE I. HIGH-ALTITUDE VEHICLE RELATED TECHNICAL PARAMETERS

Parameters	Value
Maximum height of platform (m)	12.36
Maximum operating radius (m)	5.59
Maximum angle of telescopic arm (°)	72
Maximum angle of folding arm (°)	72

III. Stress Analysis of Telescopic Arm

The structure of high-altitude vehicle is complex, especially the double parallelogram luffing mechanism of the folding arm. The stress calculation is important in order to ensure the security of operation.

International Journal of Advancements in Mechanical and Aeronautical Engineering – IJAMAE 2018

Volume 5 : Issue 2- [ISSN : 2372-4153] - Publication Date: 28 December, 2018

A. *The Structure of Telescopic ArmThe telescopic arm of high-altitude vehicle is consist of a basic arm and a primary arm, and the force analysis of the telescopic arm is shown in Fig. 2.*

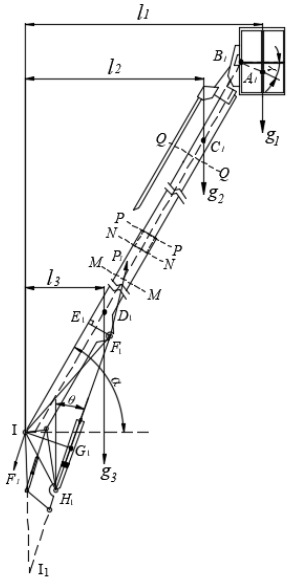

Figure 2. Force analysis of telescopic arm

B. *Stress Analysis of Basic Arm*

The template is used to format your paper and style the text. All margins, column widths, line spaces, and text fonts are prescribed; please do not alter them. You may note peculiarities.

For example, the head margin in this template measures proportionately more than is customary. This measurement and others are deliberate, using specifications that anticipate your paper as one part of the entire proceedings, and not as an independent document. Please do not revise any of the current designations.

The force analysis of the basic arm is shown in Fig. 3, and the force on the telescopic arm's cylinder is P_1, which is considered as a concentrated force.

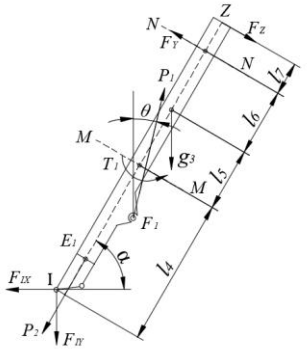

Figure 3. Force analysis of basic arm

Z is a joint point, (1) is obtained by the moment balance.

$$\begin{aligned} &F_{IY}\times(l_4+l_5+l_6+l_7)\times cos\alpha - \\ &F_{IX}\times(l_4+l_5+l_6+l_7)\times sin\alpha - \\ &P_1\times(l_5+l_6+l_7)\times cos(\alpha+\theta)+ \\ &g_3\times(l_6+l_7)\times cos\alpha - F_Y\times l_7 = 0 \end{aligned} \tag{1}$$

$$\begin{aligned} &F_Z = F_Y - P_1\times cos(\alpha+\theta)+ \\ &F_{IY}\times cos\alpha + G_3\times cos\alpha \end{aligned} \tag{2}$$

In (1) and (2), α is the angle between the telescopic arm and the horizontal direction.

According to the balance principle of force, the overall force analysis are (3), (4).

$$F_{IX} = P_1\times sin\theta \tag{3}$$

$$F_{IY} = P_1\times cos\theta - g_{23} \tag{4}$$

Sudden-changed cross-sections are dangerous sections. The dangerous sections on the basic arm are section M-M and section N-N.

The stress on the M-M section is (5).

$$\begin{aligned} &\sigma_{M-M} = \frac{M_M}{W_1}+\frac{F_M}{A_1} = \\ &\left(\begin{array}{l} F_Z\times(l_5+l_6+l_7)-F_Y\times(l_5+l_6) \\ +\frac{1}{2}\times\rho_1\times(l_5+l_6+l_7)^2\times cos\alpha+T_1 \end{array}\right)/W_1 - \\ &\rho_1\times(l_5+l_6+l_7)\times sin\alpha / A_1 \end{aligned} \tag{5}$$

The stress on the N-N section is (6).

$$\begin{aligned} &\sigma_{N-N} = \frac{M_N}{W_1}+\frac{F_N}{A_1} = \\ &\frac{F_Z\times l_7}{W_1}+\frac{\rho_1\times l_7^2\times cos\alpha}{2\times W_1}+\frac{\rho_1\times l_7\times cos\alpha}{A_1} \end{aligned} \tag{6}$$

In (5) and (6), W_1 and A_1 are the basic arm's bending section coefficient and area respectively.

The σ_{M-M} and σ_{N-N} are changed with α are shown in Fig. 4 and Fig. 5 respectively.

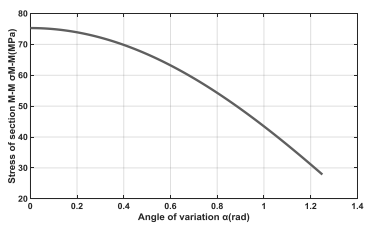

Figure 4. Sectional *M-M* stress σ_{M-M} changes with luffing angle α

International Journal of Advancements in Mechanical and Aeronautical Engineering – IJAMAE 2018
Copyright © Institute of Research Engineers and Doctors , SEEK Digital Library
Volume 5 : Issue 2- [ISSN : 2372-4153] - Publication Date: 28 December, 2018

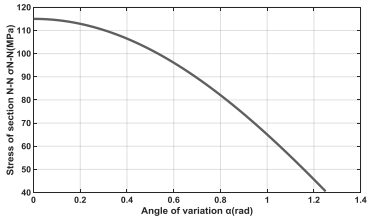

Figure 5. Sectional *N-N* stress σ_{N-N} changes with luffing angle α

From the Fig.4 and Fig5, it can be seen that the stress σ_{M-M} and σ_{N-N} decrease with the luffing angle α increase. Therefore, when α = 0, the maximum value of σ_{M-M} is 115.6MPa, and the maximum value of σ_{N-N} is 75.5MPa, which all meet the design requirements

C. *Stress Analysis of Primary Arm*

The force analysis of the primary arm of the telescopic arm is shown in Fig. 6.

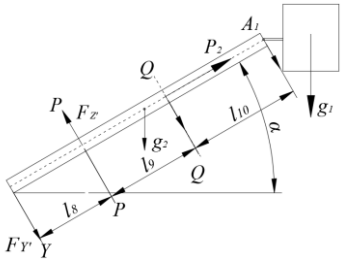

Figure 6. Primary arm force analysis

As shown in Fig. 6, the cross-section P-P and Q-Q are dangerous sections.

The stress on the P-P section is (7).

$$\sigma_{P-P}=\frac{M_P}{W_2}+\frac{F_P}{A_2}= \frac{F_Z\times l_8}{W_2}+\frac{\rho_2\times l_8^2\times cos\alpha}{2\times W_2}+\frac{\rho_2\times l_8\times cos\alpha}{A_2} \tag{7}$$

The stress on the Q-Q section is (8).

$$\sigma_{Q-Q}=\frac{M_Q}{W_2}+\frac{F_Q}{A_2}= \frac{F_Y\times(l_8+l_9)}{W_2}-\frac{F_Z\times l_9}{W_2}+\frac{\rho_2\times(l_8+l_9)^2\times cos\alpha}{2\times W_2}- \frac{\rho_2\times(l_8+l_9)\times cos\alpha}{A_2}+\frac{P_2}{A_2} \tag{8}$$

In (7) and (8), W_2 is the primary arm bending section coefficient, A_2 is the cross-sectional area., P_2 is the force of the hydraulic cylinder inside the telescopic arm.

The σ_{P-P} and σ_{Q-Q} are changed with α are shown in Fig. 7 and Fig. 8 respectively.

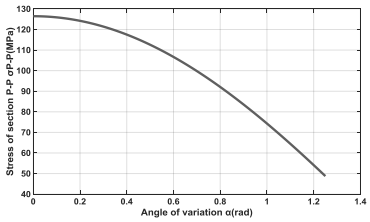

Figure 7. Sectional *P-P* stress σ_{P-P} changes with luffing angle α

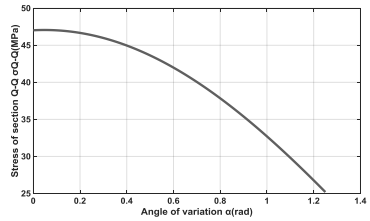

Figure 8. Sectional *Q-Q* stress σ_{Q-Q} changes with luffing angle α

From Fig. 7 and Fig. 8, it can be seen that σ_{P-P} and σ_{Q-Q} decrease with the luffing angle α. When α=0, the maximum value of σ_{P-P} is 125.6 MPa, and the maximum value of σ_{Q-Q} is 47.6 MPa., which all meet the design requirements.

IV. Stress Analysis of Folding Arm

A. *The structure of Folding Arm*

The force analysis of folding arm of the high-altitude vehicle is shown in Fig. 9.

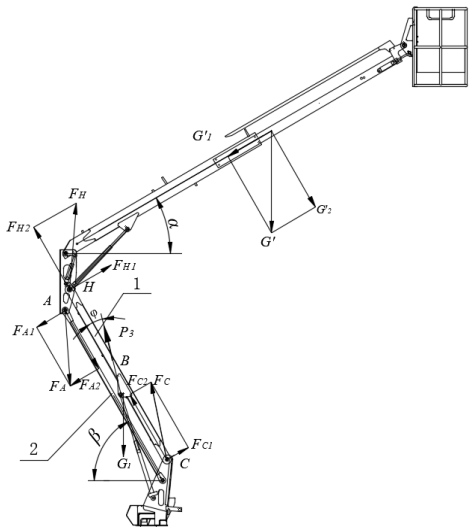

1. Main arm 2. Auxiliary arm

Figure 9. Overall force analysis of folding arm

Considering the working platform, telescopic arms, and connecting plates as a whole. The external force are put on the folding are that the overall weight G', the support force F_A at the joint point *A* and the support force F_H at the joint point *H*.

$$F_{H2} = G_2^{'} + F_{A2} \tag{9}$$

$$F_{H1} = G_1^{'} + F_{A1} \tag{10}$$

B. *Stress Analysis of Main Arm*

The main arm suffer the supporting force F_H at the joint point *H*, the hydraulic cylinder force P_3 , the supporting force F_C at the joint point *C* and the gravity of the main arm G_{OC}. The main arm is rotated to the horizontal direction is shown in Fig. 10.

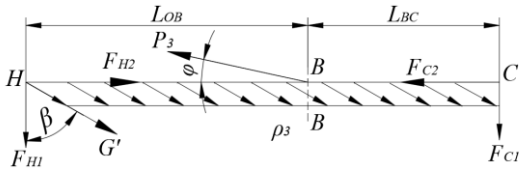

Figure 10. The force analysis of main arm at horizontal direction

The balance equations are (11) and (12).

$$F_{C1} = P_3 \times sin\varphi - F_{H1} - G^{'} \times cos\beta - G_{oc} \times cos\beta \tag{11}$$

$$F_{C2} = -P_3 \times cos\varphi + F_{H2} - G^{'} \times sin\beta - G_{oc} \times sin\beta \tag{12}$$

In (11) and (12), φ is the angle between the hydraulic cylinder and the folding arm.

The main arm is divided into two parts *HB* and *BC* at section *B-B*.

C. *Stress Analysis of* HB *Part of Folding Arm*

There is a strong mutation at section B-B, so section *B-B* is a dangerous section.

The stress in the *B-B* section is (13).

$$\sigma_{B-B} = \frac{M_B}{W_3} + \frac{F_B}{A_3} = \frac{F_{H1} \times L_{OB}}{W_3} + \frac{G^{'} \times cos\alpha \times L_{OB}}{W_3} + \frac{\rho_3^2 \times cos\beta}{2 \times W_3} + \frac{F_{H2} + G^{'} \times sin\beta + \rho_3^2 \times L_{OB} \times sin\beta}{A_3} \tag{13}$$

As shown in Fig. 11, the moment balance at the joint point C is (14).

$$M_3 = g_1 \times l_{11} + g_2 \times l_{12} + g_3 \times l_{13} - g_4 \times l_{14} - g_5 \times l_{15} + M_A \tag{14}$$

In (14), l_{11}、l_{12}、l_{13}、l_{14}、l_{15} are the arm of force to the joint point *C* respectively.

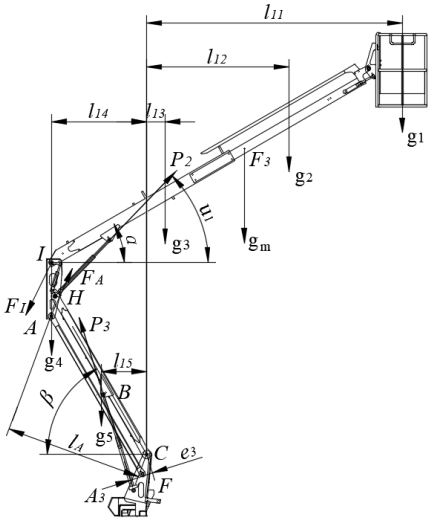

Figure 11. The luffing structure of folding arm

As shown in Fig. 12, the overall force balance equations are (15), (16).

$$F_{IX} = P_2 cos\mu_1 \tag{15}$$

$$F_{IY} = P_2 sin\mu_1 - g_m \tag{16}$$

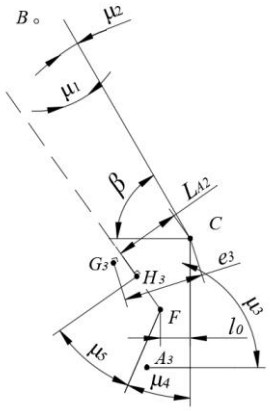

Figure 12. Bearing force of folding arm

As shown in Fig. 13, the connection is mainly affected by the torque of F_A and F_I , so the moment balance at the joint point *H* is (17).

$$F_{A2} \times l_{A2} = F_{IX} \times l_{IX} + F_{IY} \times l_{IY} + F_{A2} \times l_{A1} \tag{17}$$

$$M_A = F_{A1} \times l_{A1} + F_{A2} \times l_{A2} \tag{18}$$

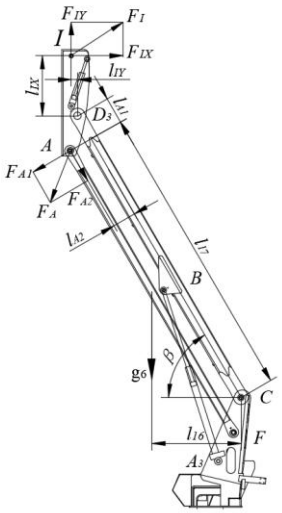

Figure 13. Force analysis of auxiliary arm

The σ_{B-B} is changed with luffing angle α and folding angel β is shown in Fig. 14 .

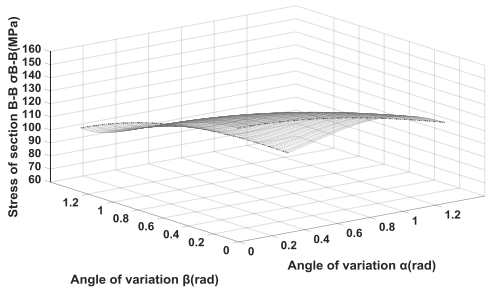

Figure 14. Sectional *B-B* stress σ_{B-B} changes with luffing angle α and folding angel β

It can be seen from Fig. 14 that the stress σ_{B-B} of the section *B-B* decreases with the angle of α and β increase, and when α =0 and β =0, the maximum value of σ_{B-B} is 147 MPa, so in order to reduce the stress value, the structural and material parameters of the arm should be modified appropriately.

D. *Stress analysis of BC part of folding arm*

As shown in Fig. 10, choosing *X-X* section as the analysis section, which is X from the *C* point $(0 \le x \le L_{BC})$.

The stress on section *X-X* is (19) and (20).

$$\sigma_{x拉} = \frac{M_x}{W_3} - \frac{F_x}{A_3} \tag{19}$$

$$\sigma_{x压} = \frac{M_x}{W_3} + \frac{F_x}{A_3} \tag{20}$$

$$M_x = F_{C1} \times x + \frac{1}{2} \times \rho_3^2 \times cos\beta \times x^2 \tag{21}$$

$$F_x = F_{C2} - \rho_3 \times sin\beta \times x \tag{22}$$

The $\sigma_{x拉}$ and $\sigma_{x压}$ are changed with luffing angle α and folding angel β are shown in Fig. 15 and Fig.16 respectively.

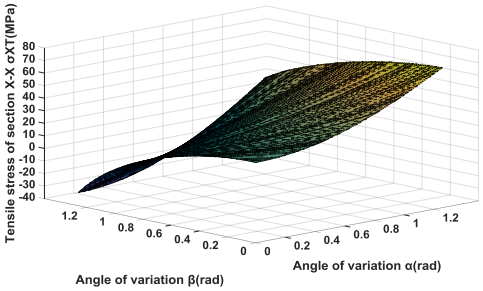

Figure 15. Sectional *X-X* stress $\sigma_{x拉}$ changes with luffing angle α and folding angel β

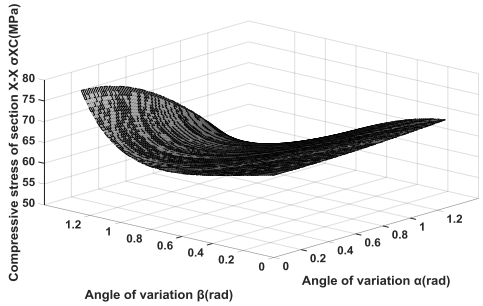

Figure 16. Sectional *X-X* stress $\sigma_{x压}$ changes with luffing angle α and folding angel β

From Fig. 15 and Fig. 16, it can be seen that when x =1.36m, α =72 and β =0, maximum value of $\sigma_{x拉}$ is 58.5MPa; and when α =0 and β =72, maximum value of $\sigma_{x压}$ is 78.5 MPa. Based on this analysis, the structural and material parameters of the arm should be modified.

E. *Force Analysis of Auxiliary Arm of The Folding Arm*

The main arm and the auxiliary arm of the folding arm constitute a parallelogram. Place the auxiliary arm on the horizon for force analysis as shown in Fig. 17.

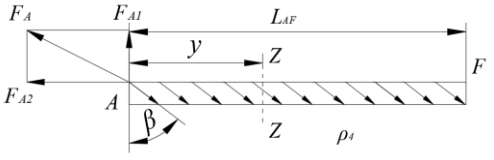

Figure 17. Force analysis of the auxiliary arm

Assuming that the distance between the *Z-Z* section and the point A is X, because the upper and lower sides of the auxiliary arm are relatively large, it is necessary to analyze them separately. And assuming the compressive stress is positive and the tensile stress is negative.

The upper and lower surface stresses on the Z-Z section are (23) and (24).

$$\sigma_{Z-Z上} = \frac{M_{Z上}}{W_4} - \frac{F_Z}{A_4} \tag{23}$$

$$\sigma_{Z-Z下} = \frac{M_{Z下}}{W_4} + \frac{F_Z}{A_4} \tag{24}$$

$$M_{Z上} = F_{A1} \times y - \frac{1}{2} \times \rho_4^2 \times y^2 \times cos\beta \tag{25}$$

$$F_x = \rho_4 \times y \times sin\beta - F_{A2} \tag{26}$$

$$M_{Z下} = -M_{Z上} \tag{27}$$

The $\sigma_{Z-Z上}$ and $\sigma_{Z-Z下}$ are changed with luffing angle α and folding angel β are shown in Fig. 18 and Fig.19 respectively.

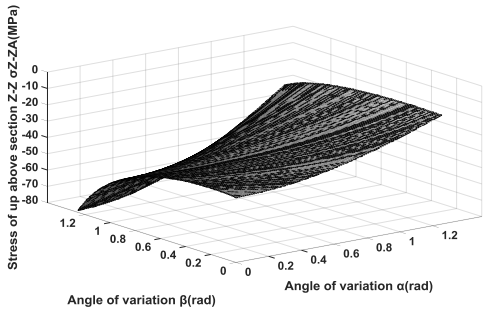

Figure 18. Sectional *Z-Z* stress $\sigma_{Z-Z上}$ changes with luffing angle α and folding angel β

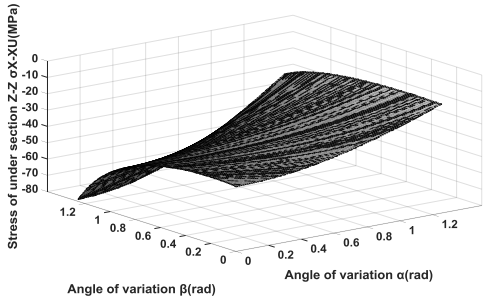

Figure 19. Sectional *Z-Z* stress $\sigma_{Z-Z下}$ changes with luffing angle α and folding angel β

From Fig. 18 and Fig. 19, it can be seen that when α =0 and β =72, the maximum of the absolute values of the stress $\sigma_{Z-Z上}$ and $\sigma_{Z-Z下}$ are 78.5 MPa and 79.5 MPa respectively, according to these stress , the structural and material parameters of the arm should be modified appropriately.

v. Conclusion

(1) Based on the mechanical analysis of high-altitude vehicle, the stress analysis of working arms is conducted.

(2) The variation curves of the relationship between the acting force of the hydraulic cylinder and the luffing angle α and the folding angle β are obtained.

(3) The method which is detail described in the paper provides a basis for structural design optimization and life prediction of high-altitude vehicle.

Acknowledgment

The research is supported by the National Natural Science Foundation of China 51475331, National Key R&D Program of China 2016YFC0802900, and also supported by the International Exchange Program for Graduate Students, Tongji University.

References

[1] J. Krasucki, A. Rostkowski, L. Gozdek, "Control strategy of the hybrid drive for vehicle mounted aerial platform," Automation in Construction, vol. 02 , pp.130-138,2009.

[2] D. Giguere, D. Marchand, "Perceived safety and biomechanical stress to the lower limbs when stepping from fire fighting vehicles," Applied Ergonomics, vol. 36 , pp. 107-119,2005.

[3] B. Hale, C. Murray, S. Douglas, "Multi-body dynamic modeling of commercial Vehicles,"Computer&Control Engineering Journal, vol. 02, pp. 11-15, 2002.

[4] R. Timothy, "An evaluation of fatigue cracking in an aerial platform yoke from a fire-fighting vehicle," Engineering Failure Analysis, vol. 09, pp. 303-312,2002

[5] Y.Hu, "Leveling mechanism for work platform on aerial vehicle",Construction Machinery and Equipment, vol. 37, pp. 34-36, December 2006.

[6] J.G.Liu, "The simualtion and optimization for variable angle mechanism of aerial platform fire truck",Jilin, Jinlin University,2011.

[7] X.L.Zhao, Q.Z. Liu, Z.G. Ma, D.Mu, "Calculation of stress of fork scissors aerial working platform", Construction Mechanization, vol. 35, pp. 36-38, August 2014.

About Author (s):

Yuxin Zheng. She was born in 1989, a doctoral student in Tongji University. Her research interests are mechanical design and multi-body dynamics.

Ying Xi. He was born in 1957, a doctoral supervisor of Tongji University, his research interests are mechanical design and simulation.

Wanghui Bu. He was born in 1982, associate professor, Tongji University, his research interests are mechanical design and mechanism analysis.